Journal of Materials Chemistry C

Accepted Manuscript

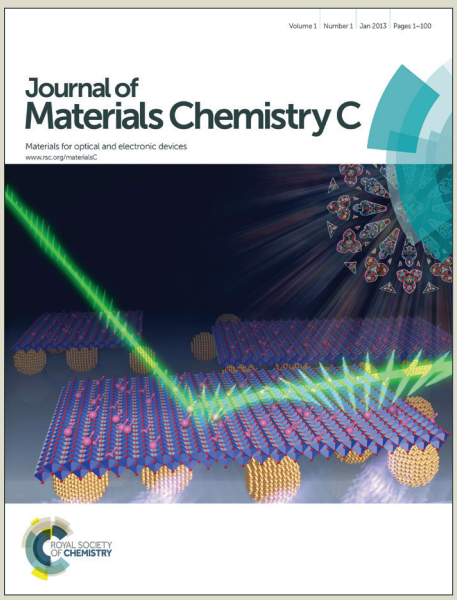

ROYAL SOCIETY OF CHEMISTRY

www.rsc.org/materialsC

Cite this: DOI: 10.1039/c0xx00000x

www.rsc.org/xxxxxx

ARTICLE TYPE

Nanofibers generated from linear carbazole-based organogelators for the detection of explosives

Guanghui Hong [a], Jingbo Sun [a], Chong Qian [a], Pengchong Xue [a], Peng Gong [a], Zhenqi Zhang [a] and Ran Lu*[a]

Received (in XXX, XXX) Xth XXXXXXXXX 20XX, Accepted Xth XXXXXXXXX 20XX
DOI: 10.1039/b000000x

Two linear carbazole-based conjugated compounds **TC3T** and **PC3P** with terminal triphenylamine and phenothiazine have been synthesized and showed selective gelation behaviors in some organic solvents upon ultrasound stimulation. SEM and TEM images of the xerogels revealed that 3D networks consisting of numerous nanofibers were formed in the gels of **TC3T** and **PC3P**. It should be noted that the obtained xerogels based on **TC3T** and **PC3P** emit strong blue and bluish green light, respectively, under UV irradiation. Upon exposed to the vapors of TNT and DNT, the emission of **TC3T** and **PC3P** in nanofibers-based films can be quenched obviously. The steady-state Stern-Volmer plots reveal that the fluorescent quenching of carbazole derivatives induced by aromatic nitro compounds is due to the photo-induced electron transfer. Therefore, the emitting nanofibers obtained from the organogelation of linear carbazoles with terminal donors can be used as fluorescent sensors to detect explosives.

Introduction

Organic nanostructures based on π-conjugated systems have attracted increasing attention in recent years due to their unique properties superior to those of the bulk counterparts, leading to promising applications in the fields of optoelectronics, nonlinear optics, photonics, chemosensors, and nanoscale devices.[1-4] It has been known that the gelation of the low molecular-weight organic π-conjugated compounds provides a strategy to create functional nano-architectures, which have been used in optoelectronic devices, light harvesting antennae, drug delivery, catalysis and template synthesis.[5-9] Among various functionalities of organic nanomaterials, the study on their sensory properties is critical for medical, environmental and security-checking purposes because the high surface-to-volume ratios associated with nanoscale chemosensors make their electrical and optical properties extremely sensitive to the analytes adsorbed on the surfaces. In particular, more effort has been made in developing various types of sensors for detection of aromatic nitro compounds, which is of importance in military operations and public security.[10-14] Till now, lots of electron-rich systems have been used as fluorescent sensory materials for probing nitroaromatics.[15] For example, Zang and Han et al have reported that the fluorescent nanofibers based on carbazole derivatives became promising sensory materials towards explosives.[16-18] In our previous work, we have found that the balanced π-π interactions favored the formation of luminescent organic nanofibers[19-22] and the emitting nanofibers based on carbazole-based trimer and pentamer as well as indolocarbazole could be used as sensory materials to detect nitroaromatics.[23,24] Herein, we intended to introduce linear tricarbazole as the building block to fulfill its gelation ability and its sensory property towards nitro compounds. On the other hand, it is found that the non-planar rigid or bulky structure in probing molecules can prevent π-stacking or the excimer formation in the excited state in the aggregates, leading to enhanced fluorescence sensory properties.[25-28] Therefore, triphenylamine and phenothiazine with non-planar configuration were employed as electron donors to functionalize linear tricarbazole, and new carbazole-based conjugated compounds **TC3T** and **PC3P** (scheme 1) were synthesized. As anticipated, **TC3T** and **PC3P** showed better gelation abilities in some organic solvents stimulated by ultrasound. From SEM and TEM images, we could find that the gelators self-assembled into 3D networks consisting

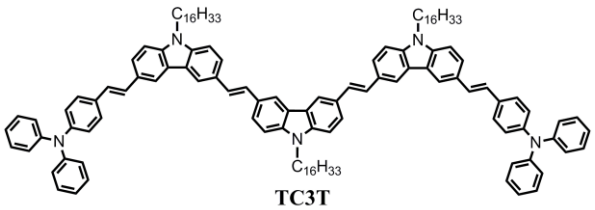

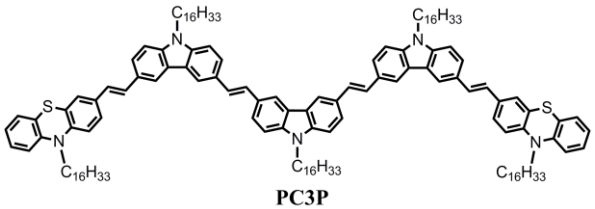

Scheme 1. Molecular structures of **TC3T** and **PC3P**.

of numerous nanofibers in gel states. It is interesting that the nanofibers formed from **TC3T** and **PC3P** were highly emissive under UV light. Upon exposed to the saturated vapors of TNT and DNT, the fluorescence emission intensity of nanofibers-based films decreased significantly. We deduced that the photo-induced electron transfer led to the fluorescent response of **TC3T** and **PC3P** towards nitroaromatics on account of the linear Stern-Volmer plots. It suggests that the organogelation of electron-rich conjugated systems provides a facile method for the fabrication of emitting nanofibers used as sensory materials to detect nitroaromatics.

Experimental

Materials

DMF was distilled from phosphorous pentoxide, and THF was freshly distilled from sodium and benzophenone. Other chemicals were used as received.

Measurements and characterizations

^{1}H NMR and ^{13}C NMR spectra were recorded with a Mercury plus instrument at 400 MHz and 125 MHz, respectively, by using $CDCl_3$ as the solvent. FT-IR spectra were measured with a Nicolet-360 FT-IR spectrometer by incorporation of samples in KBr disks. UV-vis absorption spectra were determined with a Shimadzu UV-1601PC spectrophotometer. Fluorescent emission spectra were carried out with a Shimadzu RF-5301 luminescence spectrometer. Mass spectra were performed with Agilent 1100 MS series and AXIMA CFR MALDI-TOF (matrix-assisted laser desorption ionization/time-of-flight) MS (COMPACT). Scanning electron microscopy (SEM) images was obtained on a JEOL JSM-6700F (operating at 3 kV). The samples for SEM measurement were prepared by casting the organogels on silicon wafers and dried at room temperature, followed by coated with gold. Transmission electron microscopy (TEM) experiments were performed using a JEM 3010 electron microscope (JEOL, Japan) with an acceleration voltage of 100 kV. The samples for TEM measurements were prepared by wiping a small amount of organogels onto a 300-mesh copper grid followed by natural evaporation of the solvent. Fluorescence microscopy images were taken on Fluorescence Microscope (Olympus Reflected Fluorescence System BX51, Olympus, Japan). X-ray diffraction patterns were obtained on a Japan Rigaku D/max-γA. XRD equipped with graphite monochromatized Cu Kα radiation (λ =1.5418 Å), employing a scanning rate of $0.02\,^\circ\,s^{-1}$ in the 2θ range from 2 ° to 30 °. The samples for fluorescence microscopy and XRD measurements were prepared by casting the gels on glass slide and dried at room temperature. Cyclic voltammetry was performed at room temperature under nitrogen in three electrode cells in dichloromethane containing Bu_4NPF_6 (0.1 M). The reference electrode was $Ag/AgNO_3$, the working electrode was Pt, using ferrocene as internal standard, and the scan rate was maintained at 100 mV/s on a CHI 604C voltammetric analyzer.

Synthesis of TC3T and PC3P

N,N-diphenyl-4-vinylaniline (**1**), 9-hexadecyl-6-iodo-9H-carbazole-3-carbaldehyde (**2**) 10-hexadecyl-3-vinyl-10H-phenothiazine (**5**), 9-hexadecyl-3,6-diiodo-9H-carbazole were prepared according to the methods reported previously.[19, 29-31]

(E)-6-(4-(diphenylamino)styryl)-9-hexadecyl-9H-carbazole-3-carbaldehyde (3): A mixture of compound **1** (1.45 g, 5.34 mmol), compound **2** (3.47 g, 6.36 mmol), anhydrous potassium carbonate (1.47 g, 10.68 mmol), tetrabutylammonium bromide (3.45 g) and $Pd(OAc)_2$ (20 mg) in dry DMF (30 mL) under N_2 atmosphere was stirred at 120 °C for 12 h. Then, the mixture was cooled to room temperature and poured into water (300 mL) with stirring. After extracted with CH_2Cl_2 (3 × 50 mL), the organic phase was washed with brine and dried with anhydrous magnesium sulfate. After the solvent was removed, the residue was purified by column chromatography (silica gel) using petroleum ether/ dichloromethane (v/v = 2/1) as the eluent, followed by recrystallization from the mixed solvents of dichloromethane and petroleum ether to give light yellow solid with a yield of 72%. Mp: 96.0-98.0 °C. FT-IR (KBr, cm^{-1}): 617, 691, 754, 816, 965, 1127, 1276, 1488, 1593, 1693, 2359, 2856, 2912. (Figure S26) ^{1}H NMR (400 MHz, $CDCl_3$) δ (ppm): 10.10 (s, 1H), 8.64 (d, J=4.0 Hz, 1H), 8.26 (s, 1H), 8.01 (d, J=8.0 Hz, 1H), 7.70 (d, J=8.0 Hz, 1H), 7.48-7.41 (m, 4H), 7.29-7.23 (m, 5H), 7.19 (s, 1H), 7.16-7.02 (m, 8H), 4.33 (t, J = 8.0 Hz, J = 8.0 Hz, 2H), 1.93-1.86 (m, 2H), 1.39-1.23 (m, 26H), 0.87 (t, J = 8.0 Hz, J = 8.0 Hz, 3H) (Figure S11). MALDI-TOF MS: m/z: calcd for 689.0; found: 690.2 ($[M+H]^+$) (Figure S12).

(E)-4-(2-(9-hexadecyl-6-vinyl-9H-carbazol-3-yl)vinyl)-N,N-diphenylaniline (4):

Potassium *tert*-butoxide (0.39 g, 3.48 mmol) was added to a solution of triphenylmethylphosphonium iodine (1.33 g, 3.29 mmol) in dry THF (30 mL) at 0 °C. After the mixture was stirred at room temperature for 10 min, compound **3** (1.50 g, 2.18 mmol) was added at 0 °C, and the mixture was stirred at room temperature for another 3 h. After that, the mixture was poured into water (300 mL), and extracted with CH_2Cl_2 (3 × 50 mL). The combined organic phase was washed with brine and then dried with anhydrous magnesium sulfate. After the solvent was removed, the residue was purified by column chromatography (silica gel) with petroleum ether as eluent to give light yellow solid with a yield of 90%. Mp: 92.0-94.0 °C. FT-IR (KBr, cm^{-1}): 505, 698, 741, 803, 897, 952, 1139, 1283, 1339, 1476, 1593, 2850, 2919, 3037. (Figure S27) ^{1}H NMR (400 MHz, $CDCl_3$) δ (ppm): 8.20 (s, 1H), 8.14 (s, 1H), 7.63 (d, J = 8.0 Hz, 1H), 7.57 (d, J = 8.0 Hz, 1H), 7.43 (d, J = 8.0 Hz, 2H), 7.34 (t, J = 8.0 Hz, J = 8.0 Hz, 2H), 7.28-7.23 (m, 4H), 7.19 (s, 1H), 7.14-7.01 (m, 9H), 6.95-6.88 (m, 1H), 5.78 (d, J = 16.0 Hz, 2H), 5.20 (d, J = 12.0 Hz, 2H), 4.26 (t, J = 8.0 Hz, J = 4.0 Hz, 2H), 1.87-1.82 (m, 2H), 1.36-1.23 (m, 26H), 0.87(t, J=8 Hz, J=4 Hz, 3H) (Figure S13). MALDI-TOF MS: m/z: calcd for 687.0; found: 688.0 ($[M+H]^+$) (Figure S14).

4,4'-((1E,1'E)-(6,6'-((1E,1'E)-(9-hexadecyl-9H-carbazole-3,6-diyl)bis(ethene-2,1-diyl))bis(9-hexadecyl-9H-carbazole-6,3-diyl))bis(ethene-2,1-diyl))bis(N,N-diphenylaniline) (TC3T):

A mixture of 9-hexadecyl-3,6-diiodo-9H-carbazole (0.47 g, 0.73 mmol), compound **4** (1.10 g, 1.6 mmol), anhydrous potassium carbonate (0.40 g, 2.90 mmol), tetrabutylammonium bromide (0.94 g) and $Pd(OAc)_2$ (16 mg) in dry DMF (30 mL) under N_2 atmosphere was stirred at 120 °C for 13 h. Then, the mixture was cooled to room temperature and poured into water (300 mL) with stirring. After extracted with CH_2Cl_2 (3 × 50 mL), the organic phase was washed with brine and dried with anhydrous

Cite this: DOI: 10.1039/c0xx00000x

www.rsc.org/xxxxxx

ARTICLE TYPE

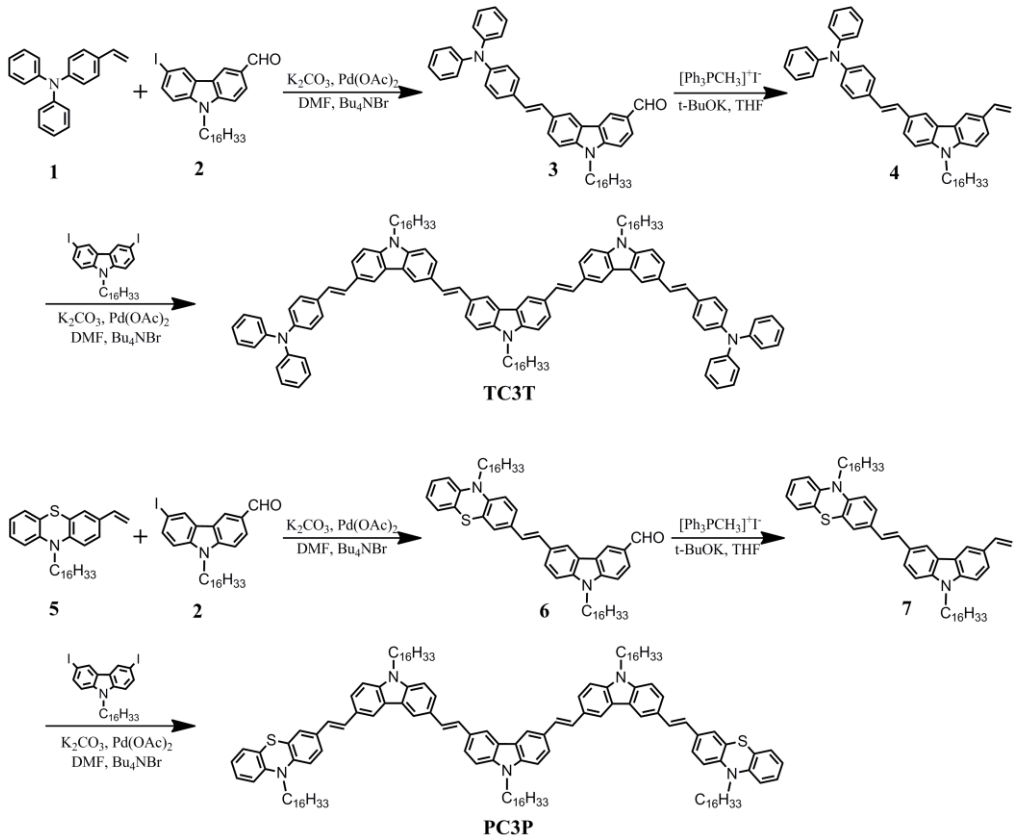

Scheme 2. The synthetic routes for **TC3T** and **PC3P**.

magnesium sulfate. After the solvent was removed, the residue was purified by column chromatography (silica gel) using petroleum ether/dichloromethane (v/v = 3/2) as the eluent, followed by recrystallization from the mixed solvents of dichloromethane and petroleum ether to give light yellow solid with a yield of 45%. Mp: 116.0-118.0 °C. FT-IR (KBr, cm^{-1}): 496, 695, 753, 798, 953, 1133, 1230, 1282, 1327, 1488, 1598, 2332, 2358, 2847, 2918. (Figure S28) ^{1}H NMR (400 MHz, $CDCl_3$) δ (ppm): 8.31 (d, J = 4.0 Hz, 4H), 8.25 (s, 2H), 7.72 (d, J = 8.0 Hz, 4H), 7.64 (d, J = 8.0 Hz, 2H), 7.45-7.35 (m, 14H), 7.27-7.21 (m, 10H), 7.13-7.00 (m, 18H), 4.28 (t, J = 8.0 Hz, J = 8.0 Hz, 6H), 1.93-1.83 (m, 6H), 1.39-1.24 (m, 78H), 0.86 (t, J = 8.0 Hz, J = 4.0 Hz, 9H) (Figure S15). ^{13}C NMR (125 MHz, $CDCl_3$) δ (ppm): 147.69, 146.78, 140.49, 140.37, 140.35, 132.42, 129.45, 129.35, 129.24, 128.94, 128.14, 127.17, 127.04, 125.58, 124.45, 124.33, 123.97, 123.35, 123.31, 122.81, 118.43, 118.30, 109.03, 43.33, 31.93, 29.71, 29.69, 29.66, 29.62, 29.59, 29.52, 29.43, 29.37, 29.08, 27.32, 22.69, 14.13 (Figure S16). MALDI-TOF MS: m/z: calcd for 1761.6; found: 1761.8 (M^+) (Figure S17).

(E)-9-hexadecyl-6-(2-(10-hexadecyl-10H-phenothiazin-3-yl)vinyl)-9H-carbazole-3-carbaldehyde (6):

A mixture of compound **2** (1.30 g, 2.89 mmol), compound **5** (1.89 g, 3.46 mmol), anhydrous potassium carbonate (0.80 g, 5.80 mmol), tetrabutylammonium bromide (1.86 g) and $Pd(OAc)_2$ (20 mg) in dry DMF (30 mL) under N_2 atmosphere was stirred at 120 °C for 12 h. Then, the mixture was cooled to room temperature and poured into water (300 mL) with stirring. After extracted with CH_2Cl_2 (3 × 50 mL), the organic phase was washed with brine and dried with anhydrous magnesium sulfate. After the solvent was removed, the residue was purified by column chromatography (silica gel) using petroleum ether/ dichloromethane (v/v = 3/2) as the eluent, followed by recrystallization from the mixed solvents of dichloromethane and petroleum ether to give light yellow solid with a yield of 78%. Mp: 66.0-68.0 °C. FT-IR (KBr, cm^{-1}): 654, 735, 803, 872, 952, 1126, 1239, 1357, 1469, 1587, 1625, 1687, 2359, 2844, 2912. (Figure S29) ^{1}H NMR (400 MHz, $CDCl_3$) δ (ppm): 10.11 (s, 1H), 8.63 (m, 1H), 8.24 (s, 1H), 8.02 (d, J = 8.0 Hz, 1H), 7.68 (d, J = 8.0 Hz, 1H), 7.48-7.41 (m, 2H), 7.35-7.29 (m, 2H), 7.16-6.90 (m, 7H), 4.33 (t, J = 8.0 Hz, J = 8.0 Hz, 2H), 3.86 (t, J = 8.0 Hz, J = 8.0 Hz, 2H), 1.91-1.81 (m, 4H), 1.44-1.23 (m, 52H), 0.87 (t, J = 8.0 Hz, J = 8.0 Hz, 6H) (Figure S18). MALDI-TOF MS: m/z: calcd for 867.3; found: 868.0 ($[M+H]^+$) (Figure S19).

(E)-10-hexadecyl-3-(2-(9-hexadecyl-6-vinyl-9H-carbazol-3-yl)vinyl)-10H-phenothiazine (7):

The synthetic method for compound **7** was similar to that of **4**

except using compound **6** (1.90 g, 2.18 mmol) as reagent. The residue was purified by column chromatography (silica gel) with petroleum ether as eluent to give bright yellow solid with a yield of 93%. Mp: 36.0-38.0 °C. FT-IR (KBr, cm^{-1}): 549, 741, 803, 878, 952, 989, 1034, 1139, 1245, 1339, 1463, 1625, 2333, 2850, 2924. (Figure S30) ^{1}H NMR (400 MHz, $CDCl_3$) δ (ppm): 8.18-8.13 (m, 2H), 7.62-7.56 (m, 2H), 7.35-7.29 (m, 4H), 7.18-7.13 (m, 3H), 7.04-6.82 (m, 5H), 5.78 (d, J = 20.0 Hz, 1H), 5.21 (d, J = 12.0 Hz, 1H), 4.26 (t, J = 8.0 Hz, J = 8.0 Hz, 2H), 3.84 (t, J = 8.0 Hz, J = 8.0 Hz, 2H), 1.87-1.78 (m, 4H), 1.44-1.23 (m, 52H), 0.87 (t, J = 8.0 Hz, J = 4.0 Hz, 6H) (Figure S20). MALDI-TOF MS: m/z: calcd for 865.4; found: 866.4 ($[M+H]^+$) (Figure S21).

3,3'-((1E,1'E)-(6,6'-((1E,1'E)-(9-hexadecyl-9H-carbazole-3,6-diyl)bis(ethene-2,1-diyl))bis(9-hexadecyl-9H-carbazole-6,3-diyl))bis(ethene-2,1-diyl))bis(10-hexadecyl-10H-phenothiazine) (PC3P):

The synthetic method for **PC3P** was similar to that of **TC3T** except using compound **7** (1.39 g, 1.60 mmol) as reagent. The crude product was purified by column chromatography (silica gel) using petroleum ether/dichloromethane (v/v = 3/2) as the eluent, followed by recrystallization from the mixed solvents of dichloromethane and petroleum ether for three times and bright yellow solid was obtained in a yield of 48 %. The obtained solid is a bit sticky. FT-IR (KBr, cm^{-1}): 598, 741, 797, 872, 952, 1133, 1245, 1339, 1463, 1488, 1625, 2359, 2850, 2924. (Figure S31) ^{1}H NMR (400 MHz, $CDCl_3$) δ (ppm): 8.32 (d, J = 12.0 Hz, 4H), 8.25 (s, 2H), 7.73 (d, J = 8.0 Hz, 4H), 7.63 (d, J = 8.0 Hz, 2H), 7.41-7.29 (m, 14H), 7.21-7.02 (m, 8H), 6.90-6.82 (m, 6H), 4.28 (t, J = 8.0 Hz, J = 8.0 Hz, 6H), 3.81 (t, J = 8.0 Hz, J = 8.0 Hz, 4H), 1.90-1.78 (m, 10H), 1.41-1.24 (m, 130H), 0.87 (t, J = 8.0 Hz, J = 8.0 Hz, 15H) (Figure S22). ^{13}C NMR (125 MHz, $CDCl_3$) δ (ppm): 144.87, 143.88, 140.53, 140.39, 140.36, 132.67, 129.50, 129.38, 128.82, 128.10, 127.41, 127.19, 127.14, 127.07, 125.40, 125.00, 124.84, 124.68, 124.43, 123.40, 123.37, 123.33, 122.34, 118.43, 118.32, 118.29, 115.48, 115.41, 109.04, 109.00, 53.37, 47.70, 43.33, 31.91, 29.69, 29.67, 29.65, 29.61, 29.57, 29.55, 29.53, 29.51, 29.50, 29.42, 29.41, 29.35, 29.25, 27.32, 27.30, 26.94, 26.88, 22.67, 14.08 (Figure S23). MALDI-TOF MS: m/z: calcd for 2118.3; found: 2117.9 (M^+) (Figure S24).

Fabrication of the nanofibers-based films for sensory investigations

Preparation of the nanofibers-based films: The solutions of **TC3T** in cyclohexane, and **PC3P** in *n*-hexane were obtained by heating. After the hot solutions were suffered a sonification for 15 s, followed by aging for several minutes at room temperature, the gels were formed. Then, diluting the gels into a "poor" solvent, such as ethanol, well-dispersed nanofibers were produced. The mesh-like film was fabricated after casting the nanofibers in "poor" solvent onto the substrate, followed by the natural evaporation of the solvent.

Stern-Volmer measurements: In steady-state emission, the quenching data fit the Stern-Volmer model well. $I_0/I = 1+K_{sv}[Q]$, where I_0 and I are the fluorescence emission intensities of the sensory material before and after adding of the quencher, respectively, and [Q] is the concentration of the quencher. Because of the absorption of the excited light by the analysts of TNT and DNT, the data in the Stern-Volmer measurements were corrected by the reported method.[32] The constant K_{sv} defines the efficiency of quenching. The sensitivity of **TC3T** and **PC3P** towards TNT, DNT was recorded by micro-titration in toluene. The concentration of **TC3T** and **PC3P** was maintained at 1.0×10^{-6} M, and the fluorescence intensity was monitored at 427 nm and 488 nm, respectively.

Sensing performance of **TC3T** and **PC3P** in the nanofibers-based film: The sensing performance of **TC3T** and **PC3P** in the nanofibers-based films towards vapor nitro compounds was studied in a way adopted by Swager and others.[15] Specifically, the film to be tested was inserted into a sealed vial at 40 ℃ containing an analyte and cotton gauze which prevents the direct contact of the film and the analyte, and helps to maintain a constant vapor pressure. The time-dependent fluorescence spectra of the film were measured after immersing the film into the sealed vial for a certain time. By monitoring the changes of the fluorescence intensity (λ_{em} = 456 nm and λ_{em} = 479 nm for **TC3T** and **PC3P**, respectively) of the film with increasing the exposure time to vapor-phase analyte, the time-dependent fluorescence quenching efficiency was obtained.

Results and discussion

Synthesis of carbazole-based compounds TC3T and PC3P

The synthetic routes for linear tricarbazole with terminal triphenylamine **TC3T** and phenothiazine **PC3P** were shown in Scheme 2. Firstly, compounds **1**, **2**, **5**, and 9-hexadecyl-3,6-diiodo-9H-carbazole were prepared according to the procedures previously reported.[19,29-31] The Heck reaction between compounds **1** and **2** catalyzed by $Pd(OAc)_2$ afforded compound **3** in 72% yield, which was transferred into compound **4** via Wittig reaction with triphenylmethylphosphonium iodine in a yield of 90%. The linear tricarbazole with terminal triphenylamine **TC3T** was prepared from compounds **4** and 9-hexadecyl-3,6-diiodo-9H-carbazole under Heck reaction condition in a yield of 45 %. Similarly, compound **6** was synthesized from compounds **2** and **5** through Heck reaction in a yield of 78%, and compound **7** was obtained from compound **6** via Wittig reaction. The Heck reaction of compound **7** with 9-hexadecyl-3,6-diiodo-9H-carbazole afforded linear tricarbazole with terminal phenothiazine **PC3P** in a yield of 48%. The new compounds were characterized by ^{1}H NMR, ^{13}C NMR spectroscopy, FT-IR and MALDI-TOF mass spectrometry. The target molecules exhibited vibration absorption bands around 952 cm^{-1} arising from the wagging vibration of the trans-double bond (C=C) in the FT-IR spectra. In addition, the ^{1}H NMR spectra of **TC3T** and **PC3P** confirmed that all the vinyl groups adopted the trans-conformation on account of the absence of the signal at ~6.5 ppm assigned to the protons in cis-double bonds (CH=CH).[29,33] Moreover, we found that the target molecules of **TC3T** and **PC3P** were soluble in toluene, xylene, and CH_2Cl_2, etc.

Photophysical and electrochemical properties of TC3T and PC3P

As shown in Figure 1a, compounds **TC3T** and **PC3P** exhibited similar absorption spectra in CH_2Cl_2. The absorption bands of **TC3T** appeared at 258 nm, 330 nm and 376 nm with a shoulder at ca. 400 nm (Table S1). The absorption at 258 nm might due to π-π* transition, and the other ones might come from n-π* transition. Similarly, **PC3P** gave three absorption bands at 267

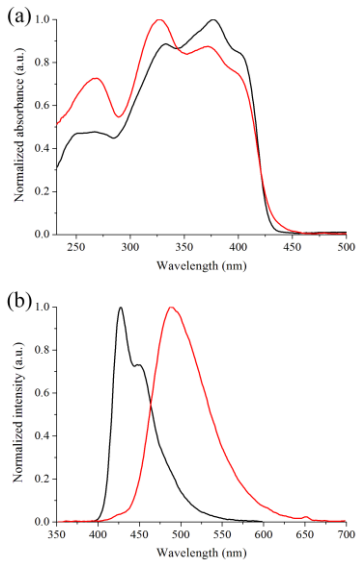

Figure 1. Normalized UV-vis absorption (a) and fluorescent emission (b, λ_{ex} = 376 nm) spectra of **TC3T** (black), **PC3P** (red) in CH_2Cl_2 (1.0×10^{-6} M).

nm, 332 nm and 371 nm with a shoulder at ca. 400 nm. As shown in Figure 1b, **TC3T** exhibited two emission bands at 427 nm and 449 nm, and only one emission band at 488 nm was detected for **PC3P** in CH_2Cl_2 (1.0×10^{-6} M). It was clear that the emission band for **PC3P** was very broad and gave an obvious red-shift compared with that for **TC3T**. On the one hand, we could ascribe the emission at 488 nm to the electronic transition of isolated instead of aggregated **PC3P** because the normalized fluorescence emission spectra of **PC3P** were quite similar at the concentrations of 1.0×10^{-7} M, 1.0×10^{-6} M, 1.0×10^{-5} M and 1.0×10^{-4} M (Figure S1a). Meanwhile, we found a linear increase of absorbance at 326 nm when the concentrations were in the range of 1.0×10^{-7} M ~ 1.0×10^{-5} M (Figure S1b). On the other hand, we obtained the solvent-dependent fluorescence emission spectra of **PC3P** and **TC3T** (Figure S2). It was found that the emission bands of both **PC3P** and **TC3T** red-shifted with increasing the polarities of the solvents, but the shift values for **PC3P** were larger than that for **TC3T**. It suggested that the large Stocks shift of **PC3P** compared with **TC3T** might be due to its more twisted configuration in the excited state.[34] The fluorescence quantum yields of **TC3T** and **PC3P** in CH_2Cl_2 were 0.38 and 0.26 using quinine sulfate in 0.1 H_2SO_4 (Φ_F = 0.55) as the standard, meaning they were high emissive in solution. Moreover, **TC3T** and **PC3P** emitted strong blue and bluish green light in apolar solvents irradiated by UV light (inset of Fig. 4b and Fig. 4d).

The electrochemical behaviors of **TC3T** and **PC3P** were investigated by cyclic voltammetry. As showed in Figure S3 and S4, it was clear that **TC3T** and **PC3P** gave one well-defined reversible oxidation peak with half-wave potential of 0.35 V and 0.26 V *vs* ferrocenium/ferrocene (Fc/Fc^+). The redox potential of Fc/Fc^+, which possesses an absolute energy level of 4.8 eV relative to the vacuum level for calibration, is located at 0.32 eV in our case. Therefore, the HOMO energy levels of **TC3T** and **PC3P** were calculated to be -4.83 eV and -4.74 eV with regard to ferrocene, respectively. Because no clear reduction peaks were observed, the LUMO energy levels of **TC3T** and **PC3P** were deduced to be -1.93 eV and -1.86 eV from HOMO energy levels and energy gaps determined by the onset of their absorption spectra. The corresponding data were summarized in Table S1. Considering the LUMO levels for TNT (-3.49 eV) and DNT (-2.98 eV),[35] the electrochemical data and strong fluorescence emission of **TC3T** and **PC3P**, we deduced that **TC3T** and **PC3P** would be candidates as fluorescence chemosensors towards nitroaromatics.

Gelation abilities of TC3T and PC3P

The gelation abilities of **TC3T** and **PC3P** were tested in the selected solvents by means of the "stable to inversion of a test tube" method.[12] It was found that they were insoluble in ethanol, 1-pentanol and 1-octanol, but showed good solubility in toluene and xylene (Table 1). Notably, after a brief sonification **TC3T** could form organogels in cyclohexane and some mixed solvents, including toluene/ethanol (v/v = 3/2), 1-octanol/toluene (v/v =

Table 1. Gelation properties of **TC3T** and **PC3P** in organic solvents.

Solvent	**TC3T** (CGC)	**PC3P** (CGC)
Methanol	I	I
Ethanol	I	I
1-Octanol	I	I
Xylene	S	S
Toluene	S	S
Toluene/Ethanol(v/v=3/1)	S	—
Petroleum ether	PG	G (2.4)
Toluene/Ethanol(v/v=3/2)	G (4.6)	—
Toluene/Ethanol(v/v=5/2)	—	S
Toluene/Ethanol(v/v=5/3)	—	P
Toluene/Ethanol(v/v=2/1)	PG	—
Toluene/Methanol(v/v=1/1)	P	—
Toluene/Methanol(v/v=5/2)	—	—
Xylene/Ethanol(v/v=2/1)	S	—
1-Octanol/Toluene(v/v=5/1)	G (2.0)	—
1-Octanol/Xylene(v/v=7/2)	G (4.4)	—
Cyclohexane/Methanol(v/v=2/1)	—	P
Cyclohexane/Ethanol(v/v=1/1)	—	P
Cyclohexane/Ethanol(v/v=7/3)	—	G (4.4)
Cyclohexane	G (1.2)	S
Xylene/Methanol(v/v=1/1)	G (5.0)	—
n-Hexane	S	G (2.2)

S: soluble; I: insoluble; G: gel; PG: partial gelation; P: precipitate. CGC: critical gelation concentration (mM).

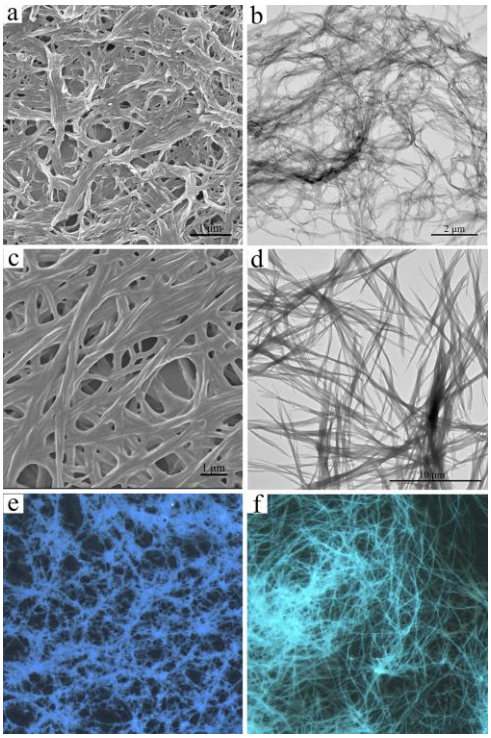

Figure 2. (a) SEM, (b) TEM and (e) Fluorescence microscopy (λ_{ex} = 330-365 nm) images of xerogel **TC3T** obtained from cyclohexane; (c) SEM, (d) TEM and (f) Fluorescence microscopy (λ_{ex} = 330-365 nm) images of the xerogel **PC3P** obtained from *n*-hexane.

5/1), 1-octanol/xylene (v/v = 7/2) and xylene/methanol (v/v = 1/1). **PC3P** could assemble into organogels upon ultrasound stimulation in *n*-hexane, petroleum ether and cyclohexane/ethanol (v/v = 7/3). The critical gelation concentrations (CGC) of **TC3T** and **PC3P** depended on the solvents varied in the range of 1.5-4.9 mM and 2.2-4.8 mM, respectively. We found that both the obtained gels were stable enough, and could not be destroyed for several weeks at room temperature.

Self-assembling properties of TC3T and PC3P in gel phases

The morphologies of the self-assemblies of **TC3T** and **PC3P** in the gel states were investigated by SEM and TEM. As shown in Figure 2a, the SEM image illustrated that 3D networks consisting of numerous nanofibers in width of tens to hundreds of nanometers and in length of tens of microns were formed in xerogel **TC3T** obtained from cyclohexane. The TEM image of xerogel **TC3T** revealed that the thinner nanofibrils could intertwist into thicker fibers (Figure 2b). Figure 2c and 2d also showed 3D networks consisting of lots of intertwined and entangled nanofibers in the xerogel **PC3P** obtained from *n*-hexane. It was clear that the nanofibers in xerogel **PC3P** were thicker, longer (hundreds of nanometers in width and tens of micrometer in length) and more straight than those in xerogel **TC3T**. It should be noted that lots of conjunctions emerged in the xerogels **TC3T** and **PC3P** as shown in SEM and TEM images, which was in accordance with their low CGC and good stability of the organogels.

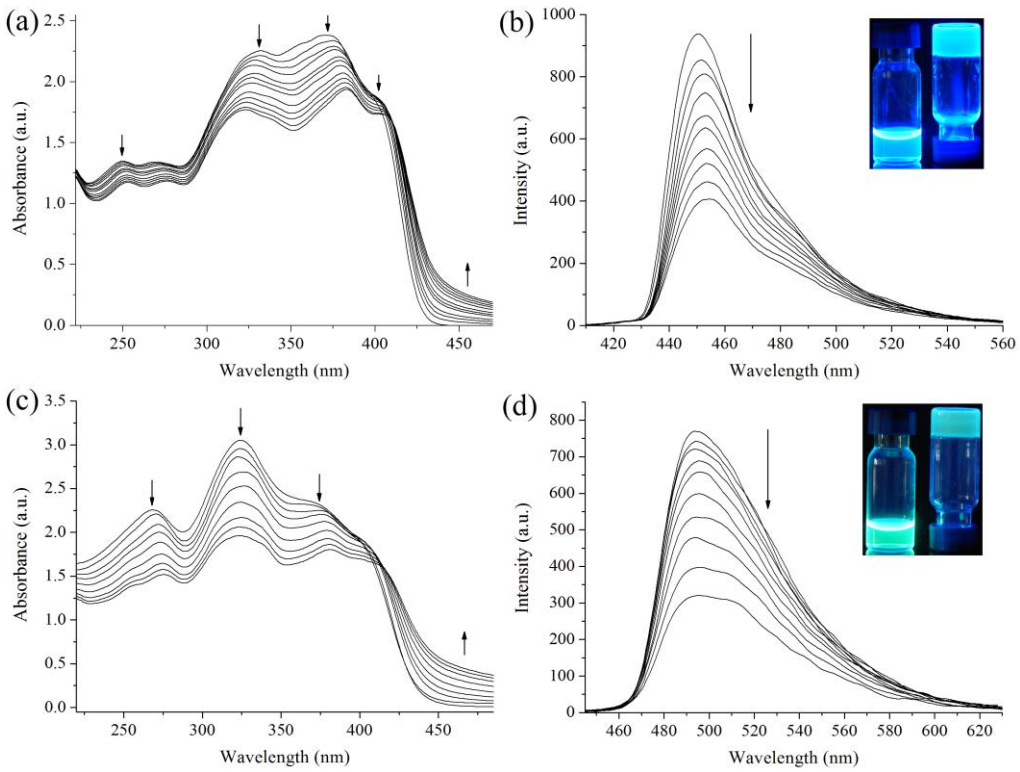

Figure 3. Time-dependent UV-vis absorption (a for **TC3T**, c for **PC3P**) and fluorescent emission (b for **TC3T**, d for **PC3P**) spectra (λ_{ex} = 376nm) of **TC3T** and **PC3P** upon cooling the hot solution in cyclohexane (1.5×10^{-3} M) and *n*-hexane (2.1×10^{-3} M), respectively, which was first stimulated by ultrasound to room temperature. The alternation is 30 s. The arrows indicate the spectral changes from the sol to gel. The insets of (b) and (d) are photographs of **TC3T** and **PC3P** in solutions (left vial) and in gel states (right vial) upon irradiated at 365 nm.

Cite this: DOI: 10.1039/c0xx00000x

www.rsc.org/xxxxxx

ARTICLE TYPE

In order to obtain the information on the self-assembling behaviors of the organogelators during the gel formation, we showed the time-dependent UV-vis absorption and fluorescent emission spectra of **TC3T** in cyclohexane and **PC3P** in *n*-hexane upon cooling the hot solutions, which were first stimulated by a brief sonification, to room temperature. As shown in Figure 3a and 3c, we could find that the absorption bands appeared in the range of ca. 220-410 nm for **TC3T** and **PC3P** decreased gradually, and new absorption in the range of above 425 nm increased gradually during the gelation process. Meanwhile, we found a concomitant red-shift of the absorption bands at ca. 249 nm, ca. 373 nm, ca. 402 nm and a blue-shift of the absorption at ca. 330 nm during the gelation of **TC3T**, and red-shift of the absorption at ca. 268 nm, at ca. 373 nm, ca. 407 nm during the gelation of **PC3P** (Figure 3c). It was found that the sol-gel transitions of **TC3T** and **PC3P** were reversible, and the absorption maximums could be recovered when the gels were destroyed into the solutions by heating. In addition, the maximal absorption bands of **TC3T** and **PC3P** red-shifted to 385 nm and 333 nm in the xerogel-based films compared with those in solutions (376 nm and 326 nm), respectively (Figure S5a and Figure S6a). Therefore, π-π interactions played an important role in the formation of the gels. Figure 3b illustrated that **TC3T** gave one broad emission band located at 450 nm in cyclohexane, whose intensity decreased gradually during the gel formation. Similarly, the intensity of the emission band of **PC3P** located at 491 nm in *n*-hexane decreased gradually during the gel formation. Although the emission of compounds **TC3T** and **PC3P** decreased upon gelation, the organogels and the obtained xerogel-based films of **TC3T** and **PC3P** still emitted strong fluorescence (insets of Figure 3b, Figure 3d and Figure 2e-f). Such aggregation-caused quenching of the emission suggested that π-aggregates formed in the gel phases.[14,36,37] The emission of **TC3T** red-shifted to 456 nm in the xerogel-based film from 427 nm in cyclohexane, and the emission of **PC3P** blue-shifted to 479 nm in the xerogel-based film from 488 nm in *n*-hexane, meaning π-π interaction took place in the xerogels. (Figure S5b and Figure S6b). Additionally, since the stretching vibration absorption for CH_2, including antisymmetric (ν_{as}) and symmetric (ν_s) stretching vibration frequencies, in the xerogel could somewhat reflected the packing conformation of alkyl chains. Therefore, we obtained the FT-IR spectrum of **TC3T** in xerogel (Figure S32), and found that the ν_{as} and ν_s absorption bands appeared at 2920 and 2850 cm^{-1}, respectively, suggesting that the alkyl chains adopted all-*trans* conformation. Thus, van der Waals and π-π interactions were the driving forces for the formation of 1D nanofibers.

The XRD pattern of xerogel **TC3T** obtained from cyclohexane showed strong Bragg reflections in the small-angle region corresponding to *d*-spacing of 2.92 nm and 1.47 nm (Figure 4a), which were close to a ratio of 1 : 1/2. We deemed that **TC3T** molecules may form layered structures in the xerogel nanofibers.[20] Moreover, the ground-state geometry of **TC3T** was optimized by AM1 calculations to reveal the molecular packing model in the gel phase. From the AM1 results a molecular width of 3.93 nm was estimated. Based on the above observations, a molecular packing model was proposed as shown in Figure 4b, in which **TC3T** molecules packed into a layered structure with π-aggregates involved. As to **PC3P**, the XRD pattern of the xerogel obtained from *n*-hexane gave two strong narrow diffraction peaks at around 2θ = 3.8 °(*d*1 = 2.28 nm) and 2θ = 10.4 °(*d*1 = 0.85 nm, Figure S7), and it is a pity that we could not deduce the molecular packing model in xerogel **PC3P**. In addition, we found one reflection peak corresponding to a *d*-spacing of 0.41 nm and 0.39 nm, respectively, for the xerogels **TC3T** and **PC3P** in the wide-

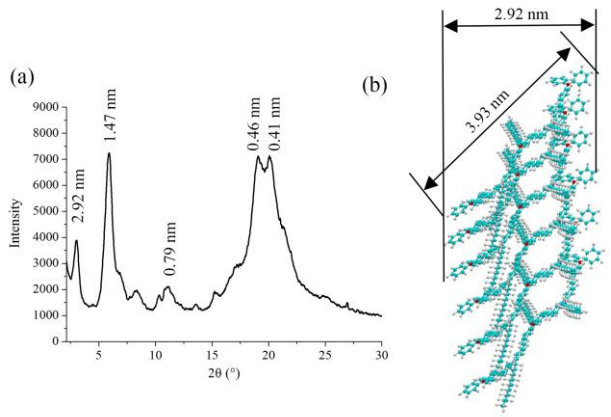

Figure 4. (a) XRD pattern of the xerogel **TC3T** obtained from cyclohexane and (b) schematic illustration of the layered structure in the gel of **TC3T** with a period of 2.92 nm.

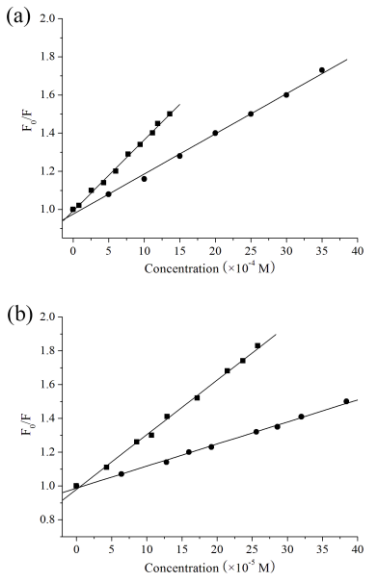

Figure 5. Stern-Volmer plots for **TC3T** (a) and **PC3P** (b) in response to TNT (square) and DNT (circle), the concentration of **TC3T** and **PC3P** was maintained at 1.0×10^{-6} M. The fluorescence intensity was monitored at 427 nm and 488 nm for **TC3T** and **PC3P** (λ_{ex} = 376 nm), respectively.

angle region of XRD patterns. It suggested that π-aggregates were formed in the gel states,[13] and the π-π interactions in xerogel **PC3P** might be stronger than that in xerogel **TC3T** due to the large bulk of triphenylamine units, which was in accordance with the results based on the absorption spectra.

Fluorescent response of TC3T and PC3P towards TNT and DNT

Based on the photophysical and electrochemical data, we could find that compounds **TC3T** and **PC3P** were electron-rich systems and gave strong emission in solutions as well as in nanofibers-based films, so we anticipated that they might be used as fluorescent sensors for probing explosives. As shown in Figure S9, it was clear that the fluorescent emission intensities of **TC3T** and **PC3P** in toluene decreased obviously upon addition of nitro compounds (TNT and DNT), and the quenching efficiencies increased gradually with increasing of the concentrations of the nitro compounds. According to the reported method,[32] Stern-Volmer plots of **TC3T** (monitored at 427 nm) and **PC3P** (monitored at 488 nm) for TNT and DNT in toluene at room temperature were shown in Figure 5, illustrating a linear fluorescence quenching response. As a result, we deemed that photo-induced electron transfer led to the fluorescent sensing of the tricarbazole derivatives towards nitro compounds. The apparent quenching constants K_{sv} was estimated by fits of the first linear part of the Stern-Volmer plots. The K_{sv} values of

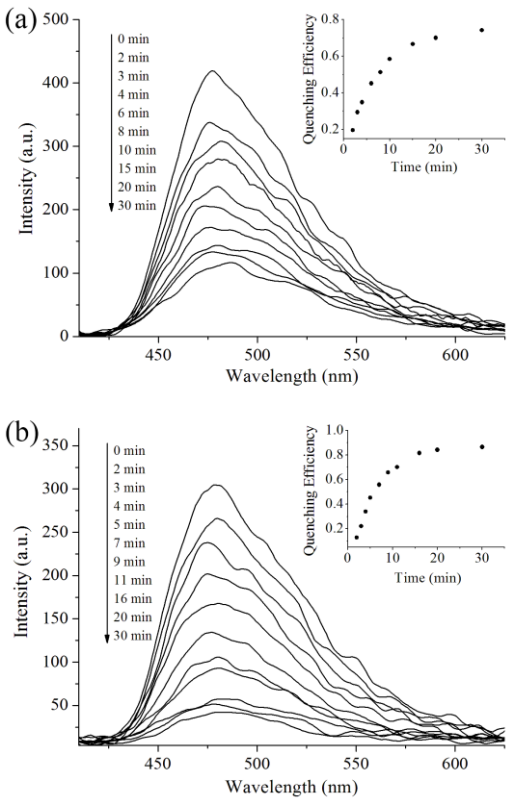

Figure 6. Time-dependent fluorescent emission spectra of the nanofibers-based film of **PC3P** (λ_{ex} = 306 nm) upon exposed to the vapors of (a) TNT and (b) DNT. The inset was the fluorescence quenching efficiency against time.

TC3T were 372 M^{-1} and 210 M^{-1} for TNT and DNT, respectively, and the K_{sv} values of **PC3P** were 3229 M^{-1} and 1307 M^{-1} for TNT and DNT, respectively. It meant that the sensitivity of the fluorescence response for **PC3P** towards TNT and DNT was higher than that of **TC3T** due to the stronger electron-donating ability of phenothiazine in **PC3P** than triphenylamine in **TC3T**.[16] It should be noted that the probes could not form aggregates in toluene when the concentration was maintained at 1.0×10^{-6} M since a linear increase of absorbance at 326 nm for **PC3P** was detected in the range of 1.0×10^{-7} M ~ 1.0×10^{-5} M (Figure S8). As a result, the electronic structures of **TC3T** and **PC3P** led to their different sensitivities towards nitroaromatics.

Moreover, the detection of vapors of nitroaromatic explosives is of vital importance in public security,[14] and it is known that the fast adsorption and diffusion as well as enhanced fluorescent quenching make the emitting nanofibers beneficial for the sensitive and fast response to gaseous analytes. Therefore, the nanofibers-based films generated from **TC3T** and **PC3P** via organogelation were employed as fluorescent sensors for detecting vapors of TNT and DNT. When the nanofibers-based films of **TC3T** obtained from cyclohexane (1.5×10^{-3} M) and **PC3P** obtained from *n*-hexane (2.1×10^{-3} M) were exposed to the vapors of TNT (0.0084 Pa)[38] and DNT (0.303 Pa)[39] at 40 ℃, the fluorescent emission intensity decreased significantly within 30 min (Figure S10 and Figure 6). The fluorescence quenching efficiency of the nanofibers-based films of **TC3T** reached 50 % and 64%, and of **PC3P** reached 74 % and 86 %, for TNT and DNT, respectively, when the exposure time was maintained at 30 min. Upon prolonging the exposure time, the fluorescent quenching rate slowed down (insets in Figure S10a-b and insets in Figure 6a-b). On the one hand, we could make the conclusion that **PC3P** in the nanofibers also exhibited more sensitive fluorescence response to nitro compounds than **TC3T**, which was similar to their sensory properties in solutions. Additionally, we found a higher fluorescence quenching efficiency of the nanofibers-based films towards gaseous DNT than TNT on account of the higher saturated vapor pressure of DNT at same temperature.[40] Moreover, we found that the quenched fluorescence of **PC3P** in the nanofibers-based film, which was first exposed to the saturated vapor of TNT (0.0084 Pa) or DNT (0.303 Pa) at 40 ℃ for 30 min, could be recovered after blown by dryer for 4 min (Figure S25), meaning that the fluorescence response of **PC3P** towards nitro compounds was reversible. These results suggested that the emitting nanofibers generated from **TC3T** and **PC3P** via organogelation could be used as fluorescent sensory materials for detecting vapor explosives.

Conclusions

In summary, we synthesized two new linear carbazole-based conjugated compounds **TC3T** and **PC3P** with triphenylamine and phenothiazine as terminal groups, which could emit strong fluorescence in solutions. It should be noted that **TC3T** and **PC3P** could form 3D networks consisting of lots of nanofibers via organogelation in some organic solvents upon ultrasound stimulations. The results of UV-vis absorption and fluorescent emission spectra changes during gelation processes as well as the XRD patterns of the xerogels revealed that π-π interactions played a key role in the gel formation. Interestingly, the

nanofibers-based films of **TC3T** and **PC3P** obtained from the organogels emitted strong fluorescence although their fluorescent intensities decreased gradually during the gel formation. Upon exposed to the vapors of the explosives of TNT and DNT, significant fluorescence quenching could be detected. Moreover, the fluorescent quenching induced by explosives could be ascribed to photo-induced electron transfer based on the linear steady-state Stern-Volmer plots of **TC3T** and **PC3P** in toluene. It provides a strategy to design and fabricate emitting nanofibers with desired functionalities via organogelation.

Acknowledgments

This work is supported by the National Natural Science Foundation of China (21374041) and the Open Project of State Key Laboratory of Supramolecular Structure and Materials (SKLSSM201407).

Notes and references

[a] *State Key Laboratory of Supramolecular Structure and Materials, College of Chemistry, Jilin University, Changchun, P.R. China. E-mail: luran@mail.jlu.edu.cn*

† Electronic Supplementary Information (ESI) available: [^{1}H NMR, ^{13}C NMR, MALDI/TOF MS, XRD, and CV spectra of target molecules; photophysical data and the changes of fluorescent emission spectra of target molecules upon addition different amount of explosives both in solution and in the nanofibers-based film]. See DOI: 10.1039/b000000x/

1 F. J. M. Hoeben, P. Jonkheijm, E. W. Meijer and A. P. H. J. Schenning, *Chem. Rev.*, 2005, **105**, 1491-1546.
2 Y. Zhao, H. Fu, A. Peng, Y. Ma, Q. Liao and J. Yao, *Acc. Chem. Res.*, 2010, **43**, 409-418.
3 B. K. An, S. K. Kwon and S. Y. Park, *Angew. Chem., Int. Ed.*, 2007, **46**, 1978-1982.
4 C. Huang, Y. Li, Y. Song, Y. Li, H. Liu and D. Zhu, *Adv. Mater.*, 2010, **22**, 3532-3536.
5 S. S. Babu, V. K. Praveen, A. Ajayaghosh. Functional π-Gelators and Their Applications; *Chem. Rev.* 2014, 114, 1973–2129.
6 Y. Liu, H. Li, D. Tu, Z. Ji, C. Wang, Q. Tang, M. Liu, W. Hu,Y. Liu and D. Zhu, *J. Am. Chem. Soc.* 2006, **128**, 12917-12922.
7 Y. Che, A. Datar, X. Yang, T. Naddo, J. Zhao and L. Zang, *J. Am. Chem. Soc*. 2007, **129**, 6354–6355.
8 H. Wang, Q. Liao, H. Fu, Y. Zeng, Z. Jiang, J. Ma and J. Yao, *J. Mater. Chem.*, 2009, **19**, 89-96.
9 S. S. Babu, V. K. Praveen and A. Ajayaghosh, *Chem. Rev.*, 2014, **114** , 1973-2129.
10 G. He, G.F. Zhang, F. Lü and Y. Fang, *Chem. Mater*., 2009, **21**, 1494-1499.
11 C. M. Yu, M. Xue, K. Liu, G. Wang and Y. Fang, *Langmuir*, 2014, **30**, 1257-1265.
12 D.T. McQuade, T.M. Swager. *Chem. Rev.*, 2000, **100**, 2537–2574.
13 S. J. George and A. Ajayaghosh. *Chem. Eur. J.*, 2005, **11**, 3217-3227.
14 S. W. Thomas, G. D. Joly and T. M. Swager, *Chem. Rev.*, 2007, **107**, 1339-1386.
15 J.-S. Yang and T.M. Swager, *J. Am. Chem. Soc.* 1998, **120**, 11864-11873.
16 C. Zhang, Y. Che, X. Yang, B. R. Bunes and L. Zang, *Chem. Commun.* 2010, **46**, 5560-5562.
17 T. Naddo, Y. Che, W. Zang, K. Balakrishnan, X. Yang, M. Yen, J. Zhao, J. S. Moore and L. Zang, *J. Am. Chem. Soc.* 2007, **129**, 6978-6979.
18 Z. C. Ding, Q. Q. Zhao, R. B. Xing, X. D. Wang, J. Q. Ding, L. X. Wang and Y. C. Han, *J. Mater. Chem. C*, 2013, **1**, 786-792.
19 X. L. Liu, X. F. Zhang, R. Lu, P. C. Xue, D. F. Xu and H. P. Zhou. *J. Mater. Chem.* 2011, **21**, 8756-8765.
20 X. F. Zhang, X. L. Liu, R. Lu, H. J. Zhang and P. Gong *J. Mater. Chem.*, 2012, **22**, 1167-1172.
21 P. C. Xue, R. Lu, P. Zhang, J. H. Jia, Q. X. Xu, T. R. Zhang, M. Takafuji and H. Ihara, *Langmuir* 2013, **29**, 417-425.
22 P. C. Xue, Q. X. Xu, P. Gong, C. Qian, Z. Q. Zhang, J. H. Jia, X. Zhao, R. Lu, A. M. Ren and T. R. Zhang, *RSC Adv*. 2013, **3**, 26403-26411.
23 G. H. Hong, C. Qian, P. C. Xue, X. L. Liu, Q. Q. Wang, P. Gong and R. Lu. *Eur. J. Org. Chem.* 2014, 6155-6162.
24 P. Gong, P. C. Xue, C. Qian, Z. Q. Zhang and R. Lu. *Org. Biomol. Chem.*, 2014, **12**, 6134-6144.
25 H. H. Nguyen, X. Z. Li, N. Wang, Z. Y. Wang, J. J. Ma, W. J. Bock and D. G. Ma. *Macromolecules* 2009, **42**, 921-926.
26 Z. H. Wang, Z. Y. Wang, J. J. Ma, W. J. Boc and D. G. Ma, *Polymer*, 2010, 842-847.
27 N. Niamnont, N. Kimpitak, K. Wongravee, P. Rashatasakhon, K. K. Baldridge, J. S. Siegel and M. Sukwattanasinitt, *Chem. Commun.* 2013, **49**, 780-782.
28 W. F. Li, H. C. Ma, and Z. Q. Lei, *RSC Adv.*, 2014, **4**, 39351-39358.
29 X. F. Zhang, X. P. Qiu, R. Lu, H. P. Zhou, P. C. Xue and X. L. Liu, *Talanta*, 2010, **82** 1943–1949.
30 Y. Zhan, K. Y. Cao, C. G. Wang, J. H. Jia, P. C. Xue, X. L. Liu, X. M. Duan and R. Lu. *Org. Biomol. Chem.*, 2012, **10**, 8701-8709.
31 T. H. Xu, R. Lu, X. L. Liu, X. Q. Zheng, X. P. Qiu and Y. Y. Zhao, *Org. Lett.*, 2007, **9**, 797-800.
32 H. Cavaye, H. Barcena, P. E. Shaw, P. L. Burn, S.-C. Lo and P. Meredith, *Proc. of SPIE*, 2009, 7418, 741803.
33 X. P. Qiu, R. Lu, H. P. Zhou, X. F. Zhang, T. H. Xu, X. L. Liu and Y. Y. Zhao, *Tetrahedron Lett.*, 2007, **48**, 7582-7585.
34 Bernard Valeur, *Molecular Fluorescence: Principles and Applications*. Wiley-VCH Verlag Gmbh, 2001.
35 G. He, N. Yan, J. Y. Yang, H. Y. Wang, L. P. Ding, S. W. Yin and Y. Fang, *Macromolecules*, 2011, **44**, 4759-4766.
36 J. B. Birks, *Photophysics of Aromatic Molecules*, Wiley, London, 1970.
37 M. Yang, D. Xu, W. Xi, L. Wang, J. Zheng, H. Zhou, J. Wu, and Y. Tian, *J. Org. Chem.*, 2013, **78**, 10344-10359.
38 J. C. Oxley, J. L. Smith, W. Luo and J. B. Propellants *Explos. Pyrotech*., 2009, **34**, 539-543.
39 A. Freedman1, P. L. Kebabian, Z. Li, W. A Robinson and J. Cwormhoudt, *Meas. Sci. Technol.*, 2008, **19**, 125102.
40 B. W. Xu, X. F. Wu, H. B. Li, H. Tong and L. X. Wang, *Macromolecules*, 2011, **44**, 5089-5092.

Graphic Abstract for:

Nanofibers generated from linear carbazole-based organogelators for the detection of explosives

Guanghui Hong [a], Jingbo Sun [a], Chong Qian [a], Pengchong Xue [a], Peng Gong [a], Zhenqi Zhang [a] and Ran Lu*[a]

Emitting nanofibers based on tricarbazole derivatives have been fabricated via organogelation and used as fluorescence sensors to detect nitroaromatics.